Proc. Indian Acad. Sci. (Chem. Sci.), Vol. 97, Nos 3 & 4, October 1986, pp. 333–347.

The adsorption of D-(+)-xylose at the mercury–water interface[§]

ROGER PARSONS* and ROBERT PEAT
Department of Chemistry, The University, Bristol BS8 1TS, England
Present address: Department of Chemistry, The University, Southampton SO9 5NH, England

Abstract. The construction of an apparatus for measuring electro capillary curves of the mercury-electrolyte interface is described based on the maximum bubble pressure technique. The adsorption of D-(+)-xylose at the mercury-aqueous 0·7953 M NaF interface is described and compared with sucrose and its isomer D-ribose.

Keywords. D-(+)-xylose adsorption; electro capillary curves; mercury-electrolyte interface; maximum bubble pressure technique.

1. Introduction

An essential feature in the understanding of electrode kinetics and double layer properties is a knowledge of the distribution of the components of the electrolyte in space and time in the vicinity of the electrode surface. In particular, emphasis has been placed on the structure of the solvent in the immediate vicinity of the electrode. The study of an organic molecule is useful in this respect as it represents the simple replacement of a layer of water adjacent to the electrode by a monolayer of an organic species. In a previous paper we have speculated from a consideration of results on a variety of polyhydroxy compounds that subtle differences in adsorption behaviour may be due to interaction of the organic species with the interfacial solvent structure (Parsons and Peat 1980). In particular sucrose lowers the interfacial tension at a mercury interface while it raises the surface tension of water and this can be attributed to a different solvent structure at the two interfaces (Frumkin 1928; Parsons and Peat 1981). Another important biological molecule that is a constituent of nucleic acids is D-ribose. The adsorption of this molecule has been studied by Brabec *et al* (1978). An isomer of D-ribose is D-xylose and the small structural change between these two molecules is manifest in the bulk solution properties. Ribose shows a marked salting in effect in the presence of sodium chloride whereas for xylose, salting out occurs (Brill 1978). This suggests a strong association between ribose and the salt. The adsorption of xylose at the mercury interface has been studied to compare its behaviour with that of sucrose and its isomer D-ribose.

[§] Dedicated to Prof. K S G Doss on his eightieth birthday.

* To whom correspondence should be addressed.

2. Experimental

Electrocapillary and differential capacitance curves were obtained for nine concentrations of D-xylose in aqueous solutions containing 0·7953 NaF as base electrolyte. The electrode potential was measured to ±0·1 mV against a 0·7953 M NaCl calomel electrode and the temperature was maintained at 25·00 ± 0·05°C. Analar NaCl and KCl were twice recrystallised from water and dried at red heat in a platinum crucible. NaF and D-xylose were BDH Analar high purity grade and were used without further purification.

Differential capacitance was measured using methods previously described (Hills and Payne 1965; Parsons *et al* 1975) and the point of zero charge was determined using a streaming electrode (Grahame 1952). All measurements were recorded at a frequency of 800 Hz and a peak to peak amplitude of 10 mV. The capacitance was independent of the frequency over the range 400–3000 Hz for all concentrations studied.

The electrocapillary curves were obtained using a high precision electrometer based on the maximum bubble pressure technique (Schiffrin 1969; Lawrence and Mohilner 1971). A consequence of the Young–Laplace equation (Adamson 1967) applied to the extrusion of a mercury drop from a capillary tube is that the interface will only be stable until the growing drop is hemispherical. Any further increase in pressure produces an unstable condition forcing the drop to grow spontaneously and break away from the tube. The pressure corresponding to the hemispherical condition is the maximum bubble pressure and is directly proportional to the interfacial tension.

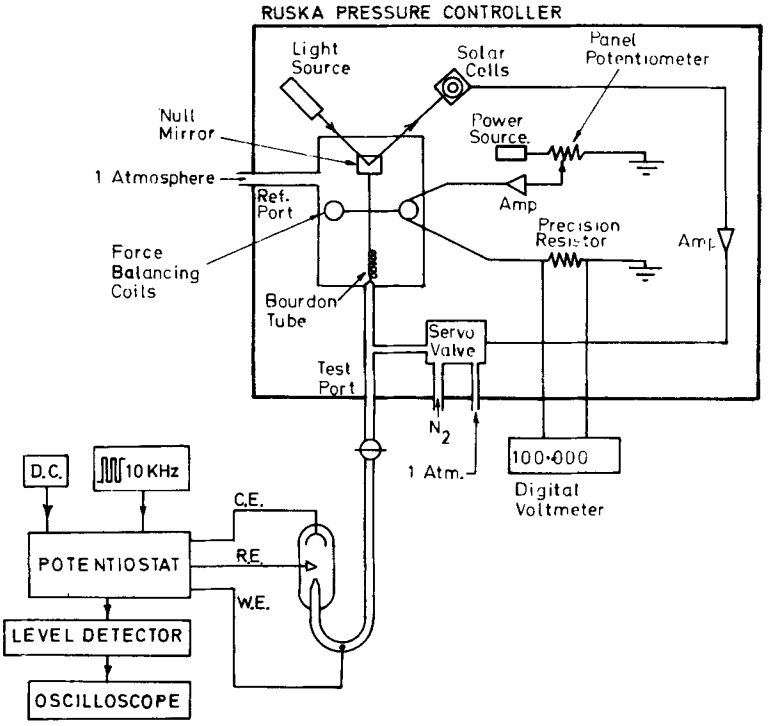

Figure 1. Schematic diagram of the maximum bubble pressure electrometer.

A schematic diagram of the electrometer is shown in figure 1. The high precision obtainable is due to the development of automatic pressure controlling equipment. The pressure system consists of a Ruska Pressure Controller (Model DDR-6000) coupled with a Datron, $5\frac{1}{2}$ digit, voltmeter (Model 1051) for the direct reading of pressure as an output voltage.

The controller consists of a chamber containing an electromagnetic coil, a quartz Bourdon tube and a null mirror. Application of a current through the coils of the tube causes movement of the null mirror. Furthermore, any movement of the mirror causes a variation in the intensity of light striking the solar cells and produces a proportional current in the external circuit. To control the pressure within the chamber, a constant current is passed through the force balancing coil by adjusting a potentiometer. The magnetic field produces a rotation of the null mirror and causes a current to flow in the external circuit. This current is amplified and used to drive a servo motor which opens a valve and lets pressurised nitrogen into the test port of the Bourdon tube. The movement of the Bourdon tube acts counter to the coils and rotates the mirror back to a null. The servo valve therefore maintains sufficient pressure in the system to balance the torque of the Bourdon tube against the torque produced by the coils. The current passing through the coils is directly proportional to the differential pressure across the Bourdon tube and is read by measuring the voltage drop across a standard precision resistor. The Bourdon tube used had a maximum differential pressure limit of 100 cm of Hg and read the pressure accurately to 0·006% of the full scale reading.

The pressure was applied to the mercury reservoir of the cell shown in figure 2. Electrical contact was made to the mercury with a platinum wire which was silver soldered to a tungsten contact fused into a side arm of the mercury reservoir. An inverted U tube capillary carried the mercury into the solution compartment of the cell. This tube was connected to the reservoir by a ball and socket joint and held secure with O rings and an aluminium clamp. This arrangement allowed a certain flexibility to the U tube and a pressure tight seal. The capillary was drawn to a diameter of 0·01 mm which is capable of supporting a mercury head of the order of 70 cm of Hg. It was upturned as this is reported to produce more reproducible results (Lawrence and Mohilner 1971; Vos *et al* 1974). The solution compartment has two optical windows allowing the capillary tip and mercury meniscus in the reservoir to be aligned with a cathetometer. The pressure, P, applied to the reservoir is then directly the pressure across the mercury-solution meniscus minus a small correction due to the hydrostatic pressure of the solution. The interfacial tension, γ, can be calculated directly from the expression:

$$\gamma = K[P - (h_{\text{soln}}\, \rho_{\text{soln}}/\rho_{\text{Hg}})] \tag{1}$$

where h_{soln} is the depth of the capillary tip below the solution/air meniscus, ρ_{soln} and ρ_{Hg} are the densities of the solution and the mercury at the temperature of the experiment and K is a calibration constant obtained from a solution of known properties. This equation should contain an expression for the density of air but the correction is negligible.

The electrode potential was controlled potentiostatically and a high frequency square wave (amplitude 5 mV peak to peak) was used to detect the maximum bubble pressure by the sudden increase in charging current that occurs as the mercury breaks away (Lawrence and Mohilner 1971). The instrument was

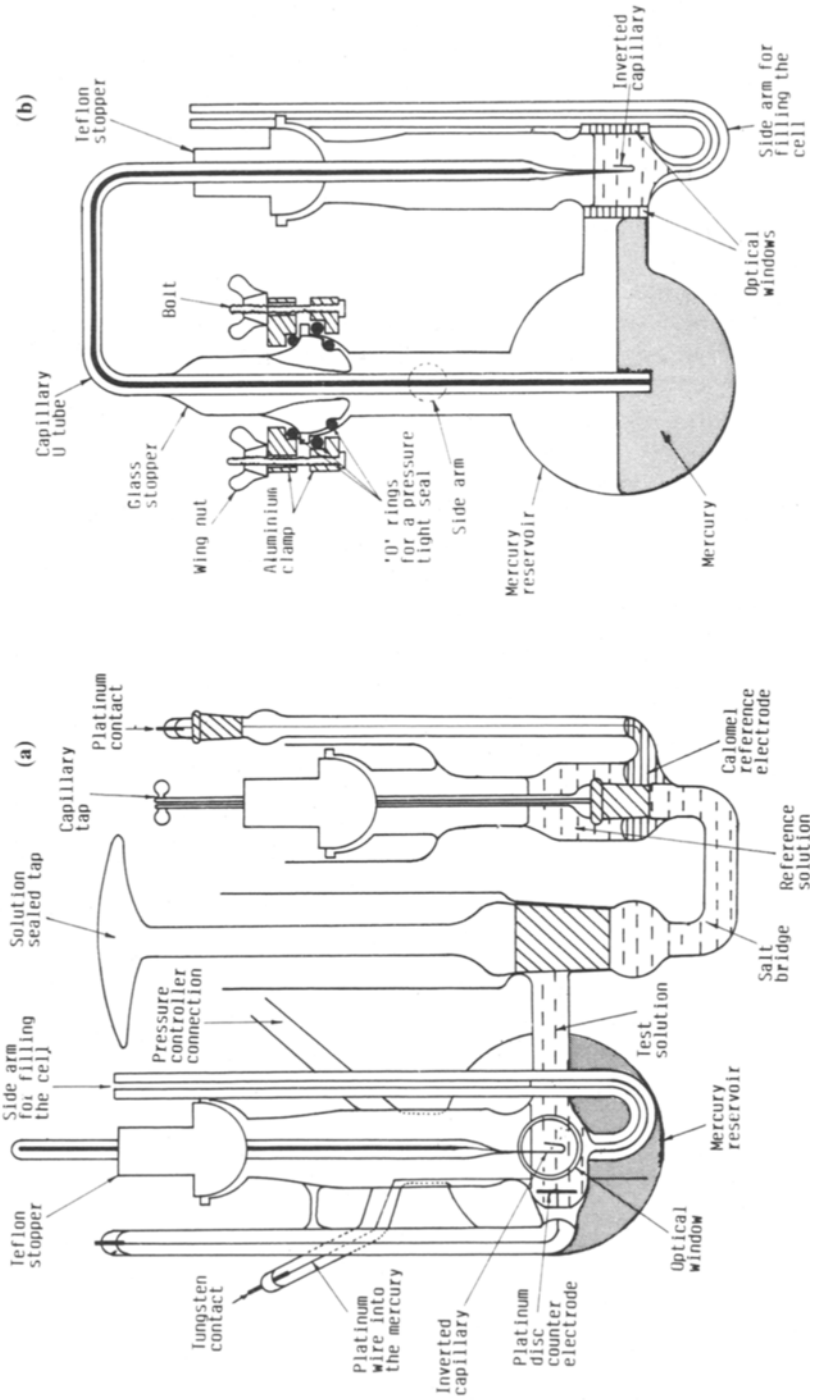

Figure 2. The electrocapillary cell (**a**) front view (**b**) left side view.

calibrated in aqueous 0·1 M KCl solution, assuming a value for the interfacial tension at the electrocapillary maximum of 426·2 mN m^{-1} (Devanathan and Peries 1954). An absolute determination by Vos and Los (1980) shows that this value is 0·6 mN m^{-1} too high. However, this leads to a proportional error of 0·15% in the derived quantities which is quite negligible. The design of the cell is such that the depth of immersion of the capillary below the solution is very small and consequently the error associated with measuring this distance becomes insignificant when converted to an equivalent mercury pressure. The variation of the density of the solution with increasing concentration of adsorbate and the increase in hydrostatic pressure due to the accumulation of mercury at the bottom of the cell are also negligible. An assessment of all errors leads to a total error on the interfacial tension of ± 0·04%, the major contribution arising from the accuracy of the pressure controller. The cell was supported on a rack in a water bath and the whole assembly was mounted on a vibration free table.

The densities of the working solutions were measured using a pycnometer that had previously been calibrated with distilled water.

3. Results and discussion

Differential capacitance curves for xylose in the concentration range 10–1000 mM are shown in figure 3. Any variation of liquid junction potentials was assumed negligible as data is not available to make the necessary corrections. The curves display features typical of an organic species with maximum adsorption occurring around the point of zero charge (PZC). The adsorption/desorption peaks are poorly defined, which is a characteristic of a weak interaction between molecules in the adsorbed layer, and desorption is incomplete at the extremes of polarisation except for the lowest concentration. At the highest concentration the adsorption is approaching saturation as demonstrated by the constant capacitance minimum at 17·20 $\mu F\ cm^{-2}$ between the potential −0·6 V to −1·05 V.

Electrocapillary curves for xylose in 0·7953 M NaCl are shown in figure 4. The rounded shape is consistent with Gouy's data (Gouy 1906) and with the poorly defined adsorption/desorption peaks displayed in the capacitance plots. The slight flattening at higher concentrations of organic compound around the pzc mirrors the capacitance minimum of figure 3. The adsorption behaviour is therefore similar in the presence of either chloride or fluoride anions. The corresponding electrocapillary curves in NaF were difficult to reproduce. These peculiarities of fluoride solutions are well documented (DeBattisti *et al* 1978) but require further detailed experimental investigation. The following analysis is based on the double integration of the capacitance curves to obtain the electrode charge and the interfacial tension. The integration constants are the point of zero charge and the interfacial tension at a known potential. The latter was obtained from the electrocapillary data by assuming that the interfacial tension measured at high negative field is independent of the anionic species. The coordinates of the point of zero charge are recorded in table 1. The charge/potential curves obtained by integration cross at a unique concentration independent potential corresponding to the position of maximum adsorption. The coordinates of this point are $\sigma^{M}_{max} = +2{\cdot}6\,\mu C\ cm^{-2}$ and $E_{max} = -0{\cdot}382$ V. This is consistent with the maximum lowering of the capacitance curve with respect to the base electrolyte.

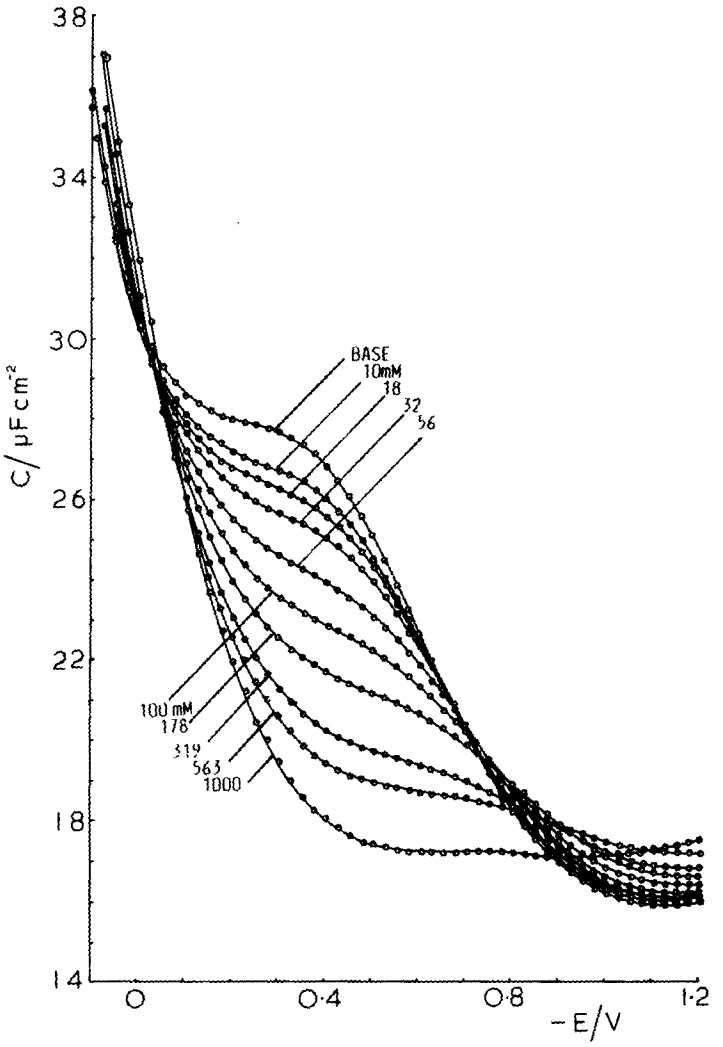

Figure 3. Differential capacity curves of a mercury electrode in contact with aqueous 0·7953 M NaF containing xylose. The concentration of xylose is indicated on each curve in mmol l^{-1}.

The surface pressure, ϕ ($= \xi_{base} - \xi$) at constant charge, was obtained from the auxiliary function $\xi (= \gamma + \sigma E)$ and the composite curve is shown as a function of concentration at the charge of maximum adsorption in figure 5. A similar curve can be obtained at constant electrode potential. The experimental scatter is of the order of $\pm 0{\cdot}3$ mN m^{-1}. Comparison of the composite isotherm with the generalised isotherms (Parsons 1961) calculated from the Frumkin equation [$\log \beta c = \log[\theta/(1-\theta] + a\theta/2{\cdot}303$] predicts a value for the interaction coefficient, a, of $-0{\cdot}25$ corresponding to a weak attractive interaction between the adsorbed molecules; the saturation coverage Γ_s was obtained from the surface coverage $\theta (= \Gamma/\Gamma_s)$ and has a value of $3{\cdot}3 \times 10^{-10}$ mol cm^2, which is

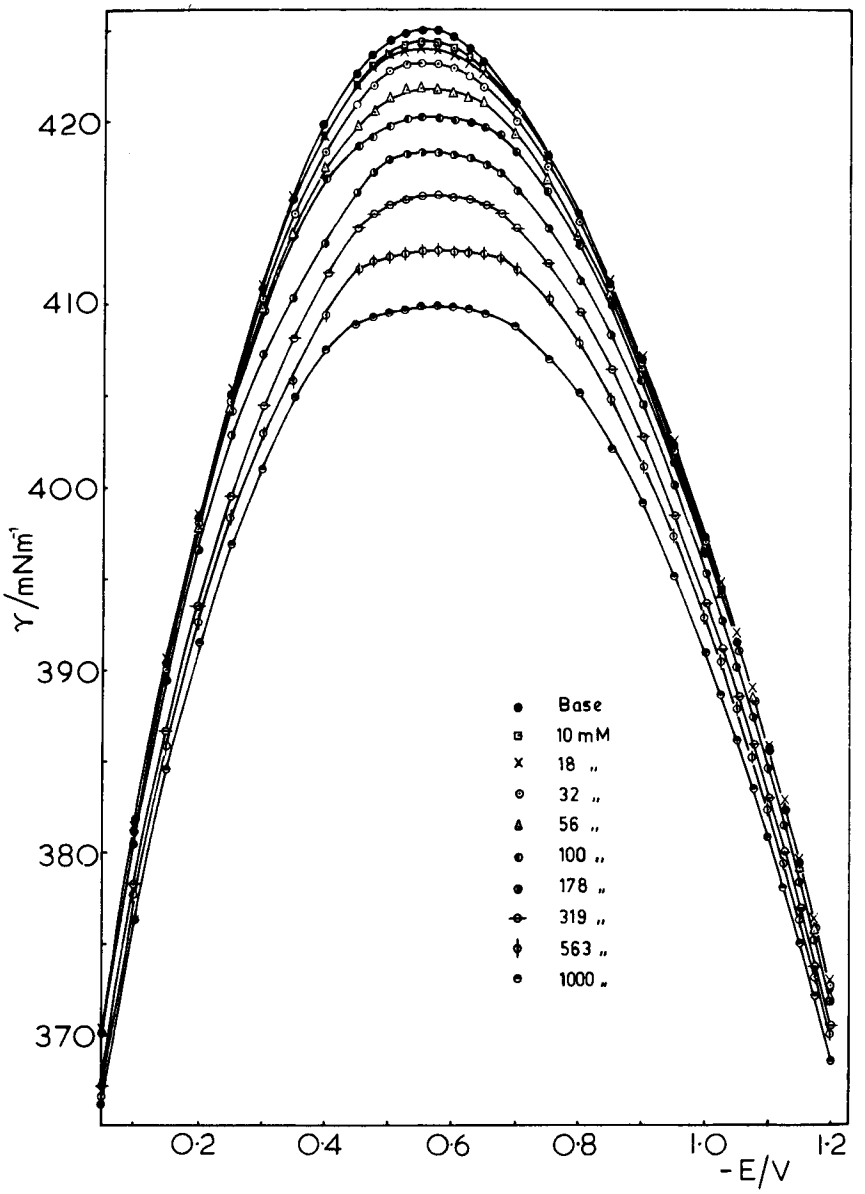

Figure 4. Electrocapillary curves for a mercury electrode in contact with aqueous 0·7953 M NaCl containing xylose.

equivalent to a molecular area of 0·5 nm^2, implying from space filling models (figure 6) that xylose is adsorbed with the plane of the ring flat on the electrode; the value of log β was +0·79. The theoretical surface pressure corresponding to these parameters is compared with experimental data in figure 7. The generalised isotherms for the Virial and Volmer equations are unable to describe the shape of composite curves. However, as previously pointed out (Krishnan and de Levie 1982) the validity of these isotherm fitting procedures must be treated with caution.

Table 1. Coordinates of the pzc of mercury in contact with 0·7953 mol l^{-1} NaF containing D-xylose at 25°C. Potentials are measured with respect to an aqueous 0·7953 mol l^{-1} NaCl calomel electrode.

c/mmol l^{-1}	$-E_{pzc}$/V	γ_{pzc}/mN m^{-1}	C_{pzc}/μF cm^{-2}
0	0·4810	428·0	25·39
10	0·4833	427·4	24·82
18	0·4850	427·2	24·52
32	0·4877	426·7	24·04
57	0·4919	425·5	23·16
100	0·4976	424·0	22·21
178	0·5039	421·7	21·15
319	0·5110	418·9	19·67
563	0·5175	415·4	18·87
1000	0·523	410·8	17·30

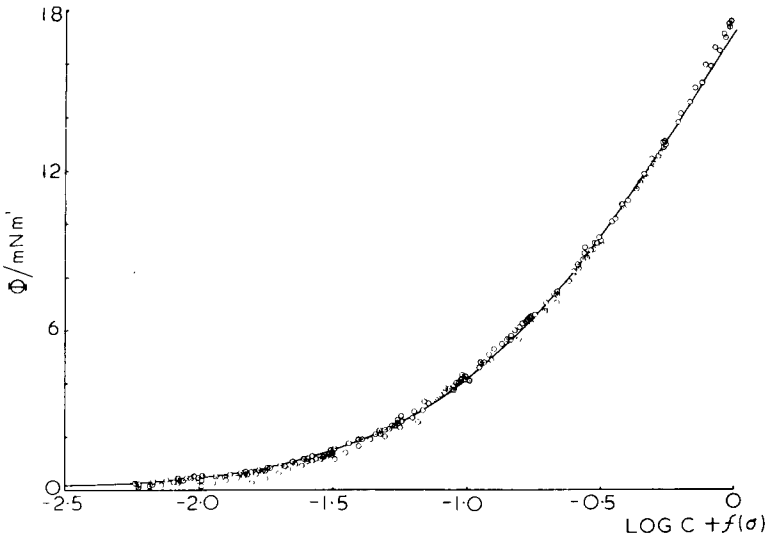

Figure 5. Composite surface pressure curve for xylose adsorbed on mercury in contact with 0·7953 M NaF at 25°C. The line was calculated from the Frumkin isotherm with $a = -0{\cdot}25$, $\Gamma_s = 3{\cdot}32 \times 10^{-10}$ mol cm^{-2}, and $\log \beta = 0{\cdot}79$.

The relative surface excess (Γ) of xylose was determined at constant charge by numerical differentiation of the function ξ with respect to the logarithm of xylose concentration. It was assumed that the activity could be approximated by the concentration, as the activity coefficients in the ternary mixture NaF + water + xylose are not available. However, some results show that xylose (Brill 1978) behaves like sucrose at these concentrations of base electrolyte and therefore, the errors introduced by the approximation are likely to be of the same order of magnitude

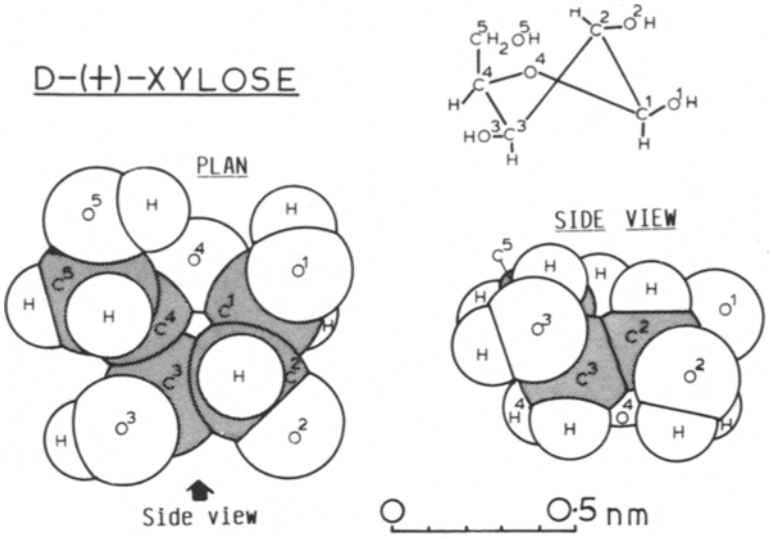

Figure 6. Schematic structure and scale drawing of a molecule of D-(+)-xylose.

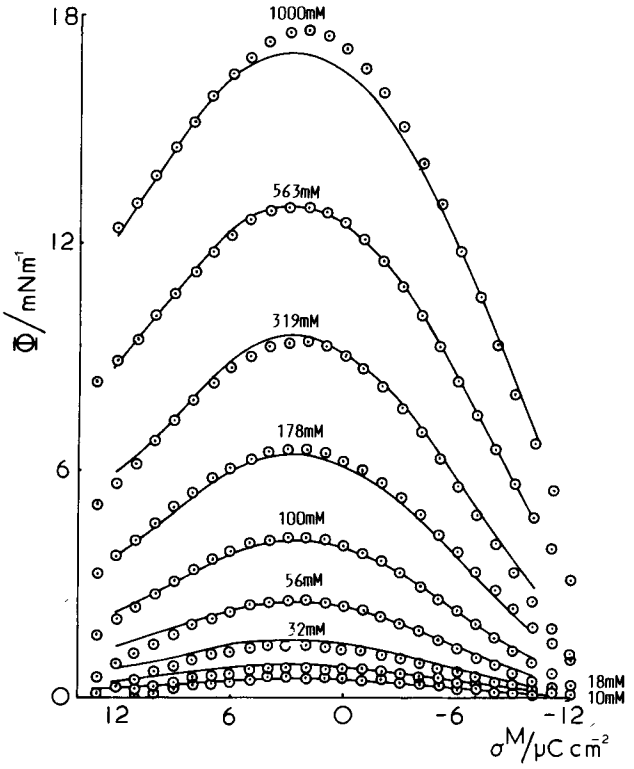

Figure 7. The surface pressure of xylose as a function of charge density on the mercury surface at 25°C. The xylose concentration in mmol l^{-1} is indicated on each curve. The lines were calculated from the Frumkin isotherm with $a = -0{\cdot}25$, $\Gamma_s = 3{\cdot}32 \times 10^{-10}$ mmol cm^{-2}, log $\beta = 0{\cdot}79$ and experimental values of $f(\sigma)$.

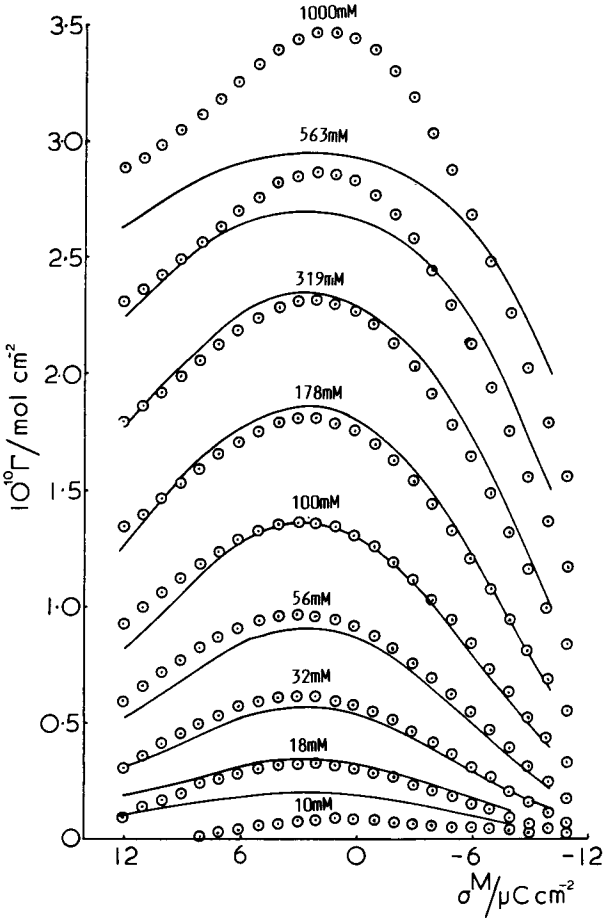

Figure 8. The relative surface excess of xylose as a function of charge density on the mercury surface at 25°C. The concentration of xylose in mmol l^{-1} is indicated by each curve. The lines were calculated from the Frumkin isotherm with $a = -0{\cdot}25$, $\Gamma_s = 3{\cdot}32 \times 10^{-10}$ mol cm^{-2}, log $\beta = 0{\cdot}79$ and experimental values of $f(\sigma)$.

(Parsons and Peat 1981) and become significant only for concentrations above 0·5 mol l^{-1}. The results are shown in figure 8. The agreement with the Frumkin isotherm is satisfactory except for the end concentrations which is probably a result of the numerical differentiation technique. The resulting data may be fitted to the Langmuir isotherm arranged in a linear form

$$c/\Gamma = c/\Gamma_s + 1/\Gamma_s\beta, \tag{2}$$

where c is the concentration of adsorbate. The linear relationship at constant charge was displayed in the concentration range 0–0·3 mol l^{-1} with parameters Γ_s of $3{\cdot}3 \times 10^{-10}$ mol cm^{-2} and log β of $+0{\cdot}84$ that agree favourably with surface pressure analysis. This is not surprising considering the low value obtained for the interaction parameter in the Frumkin equation.

The standard Gibbs energy of adsorption was calculated from the adsorption coefficient ($\log \beta = 0{\cdot}79$) by assuming that the adsorption process corresponds to a solvent displacement equilibrium. If the standard states are chosen as unit mole fraction for the adsorbate and solvent in the bulk phase and on the surface then:

$$\beta = [1/c_{s,b}]\exp(-\Delta\bar{G}^{\circ}/RT) \tag{3}$$

where $c_{s,b}$ is the bulk solvent concentration. Substituting the value of β into this equation gives $-14{\cdot}47$ kJ mol^{-1} for the standard Gibbs energy of adsorption at the point of maximum adsorption $\Delta\bar{G}^{\circ}_{max}$). This value is considerably less than the value of -22 kJ mol^{-1} for sucrose (Parsons and Peat 1981). A decrease in the standard Gibbs energy of adsorption for xylose compared to sucrose would be expected due to its smaller molecular size. This can be assumed from the work of Kaganovich and Gerovich (1966) who claim that the adsorption of aliphatic amines, acids and alcohols forming an homologous series conforms to the Traube rule. This is equivalent to the condition that the Gibbs energy is an additive function of the number of $-CH_2-$ groups in the molecule. Also Dryhurst and coworkers (Brabec *et al* 1977; Kinoshita *et al* 1977) have studied the adsorption of some nucleosides and claim from their results (Brabec *et al* 1978) that the standard Gibbs energy of adsorption is given by the sum of the standard Gibbs energy of the free base (purine or pyrimidine) with that of the free sugar (ribose or deoxyribose). Sucrose consists of D-glucose and D-fructose joined by a glycosidic linkage so a substantially smaller standard Gibbs energy might be expected for the single ring compound. However, the standard Gibbs energy is a complex quantity dependent upon metal-adsorbate, metal-solvent, adsorbate-adsorbate, adsorbate-solvent and solvent-solvent interactions in both the surface and the bulk phases. Xylose is less soluble in aqueous solution than sucrose and in this respect would be expected to be adsorbed to a greater extent. As the converse is true then the difference in behaviour of the two compounds is likely to be due to interactions within the surface phase, rather than to a difference in the energy of the molecules in solution. This may be due to a strong chemical interaction with the metal because of the presence of $-OH$ groups, although this seems unlikely as the values for the standard Gibbs energy are similar to those expected for physical adsorption. Alternatively we have argued previously in a comparison of the air/water and metal/water interfaces that there could be a specific solvent structure that is induced by the metal or the organic molecule that is favourable for the adsorption of sucrose but unfavourable for xylose (Parsons and Peat 1980). Dramatic changes in adsorption behaviour that are thought to be due to subtle changes in solvent structure have been demonstrated recently for the stereoisomers mannitol and sorbitol (Peat and Shannon 1983). D-ribose and 2-deoxy-D-ribose have been studied (Brabec *et al* 1978) and these adsorbates also show weak adsorption with the molecules adsorbed with the plane of the ring flat on the electrode surface. However, there is a distinct difference in that the D-ribose shows a maximum adsorption at -2 μC cm^{-2} compared with $+2{\cdot}6$ μC cm^{-2} for xylose. Furthermore, substitution of a single $-OH$ for a H atom in 2-deoxy-D-ribose shifts the maximum adsorption to -4 μC cm^{-2}. This is difficult to explain qualitatively from a structural aspect due to the complex molecular conformations involved but does indicate that small structural changes in the molecule can cause marked changes in adsorption behaviour.

The variation of standard Gibbs energy with electric field was determined

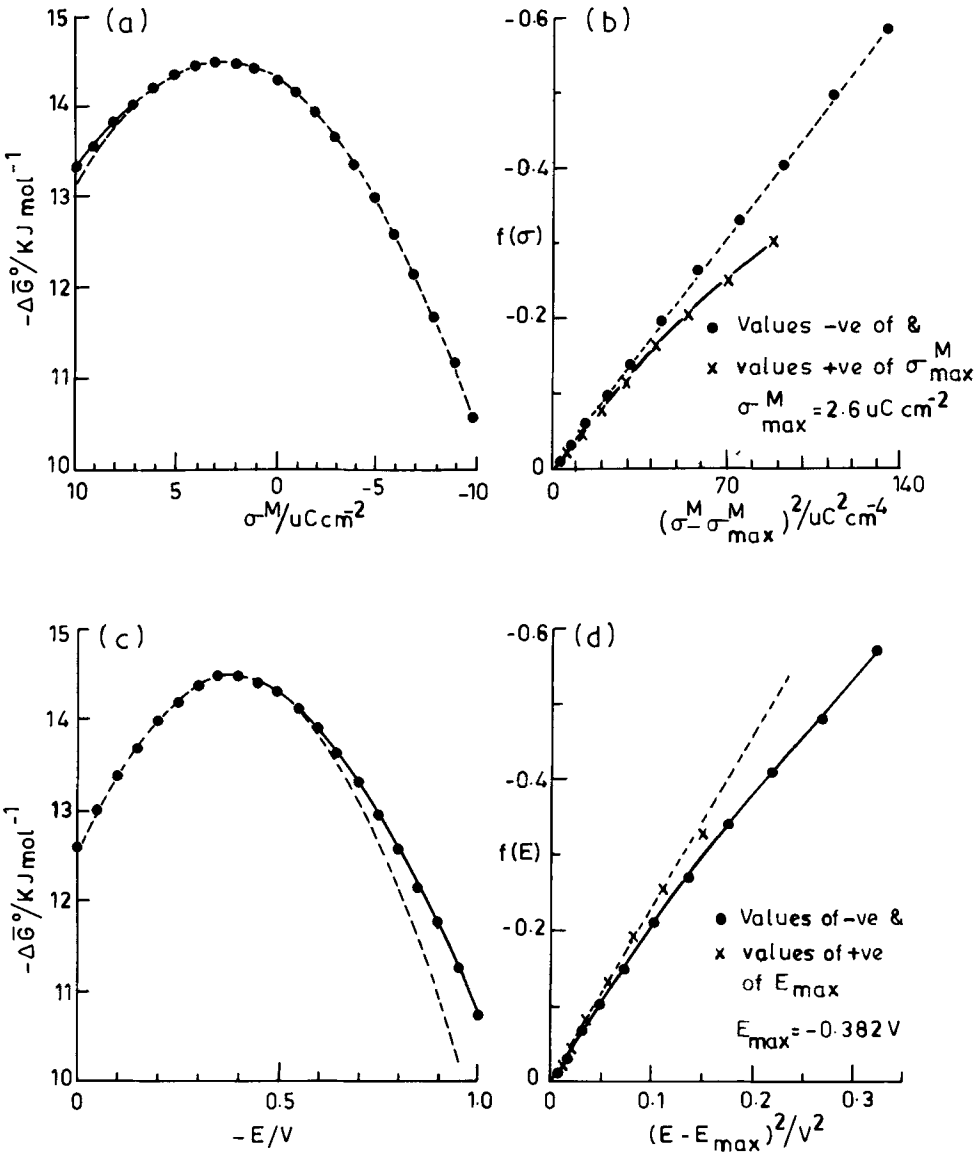

Figure 9. The variation of the standard Gibbs energy of adsorption of xylose with charge (**a**) and potential (**c**). The same data plotted as a function of $(\sigma-\sigma^M)^2$ (**b**) and $(E-E_{max})^2$ (**d**) The broken lines are calculated from (4) and (6) with $b = 0{\cdot}0043$ cm^4 μC^{-2} and $\alpha = 2{\cdot}31$ V^{-2} respectively.

experimentally from the shift to superimpose the surface pressure curves at constant electrical variable and the results are shown in figure 9. A quadratic dependence characteristic of organic adsorption was found. According to the

model of two capacities in series (Parsons 1963) the variation of standard Gibbs energy is given by

$$f(\sigma) = \log \beta - \log \beta_{max} = -b(\sigma^m - \sigma^m_{max})^2, \tag{4}$$

where

$$b = (1/2 \times 2{\cdot}303\, RT\Gamma_s) - 1\ (C_1^{-1} - C_0^{-1}), \tag{5}$$

and where C_0 is the capacity corresponding to zero coverage. This model is satisfactory in the charge range $+7$ to $-10\ \mu C\ cm^{-2}$ with $b = 0{\cdot}0043\ cm^4\ \mu C^{-2}$ (figure 9b). The alternative plot at constant potential corresponds to Frumkin's model of two capacitors in parallel for which (Parsons 1976)

$$f(E) = \log \beta - \log \beta_{max} = -\alpha(E - E_{max})^2, \tag{6}$$

where

$$\alpha = (C_0 - C_1)/2{\cdot}303\, RT\Gamma_s. \tag{7}$$

As the charge-potential curves pass through a concentration-independent point corresponding to the point of maximum adsorption, it follows that the series and parallel models coverage at this unique point and

$$\sigma^m_{max} = -E_N C_1 C_0/(C_0 - C_1) = E_{max}\ C_0, \tag{8}$$

where E_N is the shift of the point of zero charge due to the adsorption of organic compounds and E_{max} is measured with respect to the point of zero charge. Substituting the values for σ^m_{max} and E_{max} into (8) leads to a value for C_0 of $26{\cdot}24\ \mu F\ cm^{-2}$. Taking the experimental values for b and Γ_s and the calculated value for C_0 in (5), then C_1 has a value of $18{\cdot}38\ \mu F\ cm^{-2}$. Substituting σ^M_{max}, C_0 and C_1 back into (8) predicts a calculated value of $-0{\cdot}042$ V for the shift of the point of zero charge due to adsorption of the organic species. Similar conclusions can be drawn from the shift of potential caused by the adsorption of xylose which is plotted in figure 10.

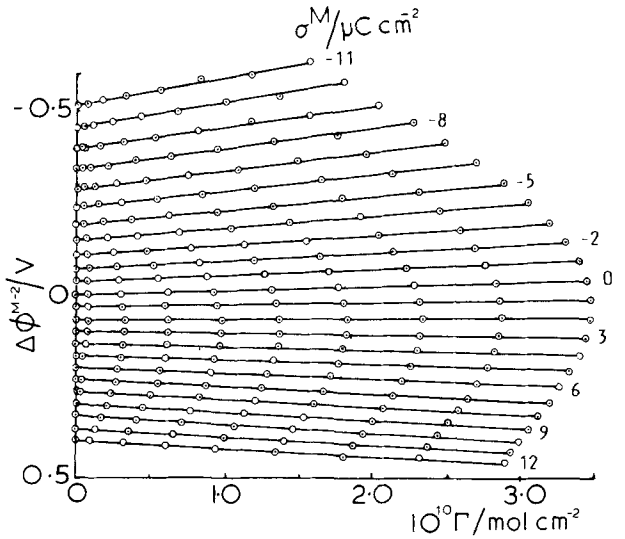

Figure 10. The change of rational potential drop across the inner layer upon adsorption of xylose at constant charge. Charge values are indicated by each curve.

Here $\Delta\phi^{m-2}$ is the change in the rational potential drop across the inner layer. It was calculated from:

$$\Delta\phi^{m-2} = E_\sigma^N - E_{\sigma=0}^{\text{base}} - \phi_\sigma^{2-s}, \tag{9}$$

where ϕ_σ^{2-s} is the diffuse layer potential drop, E_σ^N is the measured potential in the presence of adsorbate and $E_{\sigma=0}^{\text{base}}$ is the pzc of the base electrolyte. The linear relationship implies congruence of the isotherm with respect to electrode charge and the zero gradient at $+2{\cdot}6\ \mu\text{C cm}^{-2}$ corresponds to the charge of maximum adsorption. The shift of the potential of zero charge due to adsorption of a monolayer of xylose can be obtained by extrapolation of the data at $\sigma^m = 0$ to Γ_s. The value of $-0{\cdot}042$ V is in excellent agreement with the previous calculations using the capacitors in series model. Similar arguments based on the value of $\alpha = 2{\cdot}31\ \text{V}^{-2}$ from figure 9d predict a value of $-0{\cdot}050$ V for E_N which does not agree with the experimental value.

Increasing evidence suggests that water is adsorbed at the point of zero charge with its oxygen atom adjacent to the metal and that the surface potential, $g_{(M)}^{H_2O}$ (dip), is of the order of $-0{\cdot}080$ V (Trasatti 1970). The negative shift in potential upon replacing water by xylose also implies that this molecule is adsorbed with the negative end of its dipole towards the metal. At saturation coverage the shift of the point of zero charge is given by:

$$E_N = g_{(M)}^N\ (\text{dip}) - g_{(M)}^{H_2O}\ (\text{dip}) \tag{10}$$

where $g_{(M)}^N$ (dip) has the value $-0{\cdot}122$ V and is the surface dipole potential for xylose on the uncharged surface. The negative sign confirms the orientation for xylose with the negative end of its dipole towards the metal. Assuming a value for ε of 9·78 based on the thickness of the water layer as 0·33 nm and a C_0 value of 26·24 $\mu F\ \text{cm}^{-2}$ then the effective dipole moment for xylose is 5×10^{-30} c.m. This compares favourably with a dipole moment of $2{\cdot}0 \times 10^{-29}$ c.m estimated by Franks *et al* (1973) for several similar compounds in aqueous solution.

Acknowledgements

We are grateful to Drs R M Reeves and I Williams who designed and built the maximum bubble pressure electrometer and to the Science Research Council for a maintenance grant to R Peat.

References

Adamson A W 1967 *Physical chemistry of surfaces* (London: John Wiley and Sons)
Brabec V, Christian S D and Dryhurst G 1977 *J. Electroanal. Chem.* **85** 389
Brabec V, Christian S D and Dryhurst G 1978 *J. Electrochem. Soc.* **125** 1236
Brill R V 1978 *Tech. Res. Commun., Curr. Data News* **6** No. 6
DeBattisti A, Amadelli R and Trasatti S 1978 *J. Colloid Interface Sci.* **63** 61
Devanathan M A V and Peries P 1954 *Trans. Faraday Soc.* **50** 1236
Franks F, Reid D S and Suggett A 1973 *J. Solution Chem.* **2** 99
Frumkin A N 1928 *Ergeb. Exakten. Naturwiss.* **7** 564
Gouy G 1906 *Ann. Chim. Phys.* **8** 291

Grahame D C, Coffin E M, Cummings J I and Poth M A 1952 *J. Am. Chem. Soc.* **74** 1207
Hills G J and Payne R 1965 *Trans. Faraday Soc.* **61** 326
Kaganovich R I and Gerovich V M 1966 *Elektrokhimiya* **2** 977
Kinoshita H, Christian S D and Dryhurst G 1977a *J. Electroanal. Chem.* **83** 151
Kinoshita H, Christian S D and Dryhurst G 1977b *J. Electroanal. Chem.* **85** 377
Krishnan M and de Levie R 1982 *J. Electroanal. Chem.* **131** 97
Lawrence J and Mohilner D M 1971 *J. Electrochem. Soc.* **118** 259, 1596
Parsons R 1961 *Proc. R. Soc. London* **A261** 79
Parsons R 1963 *J. Electroanal. Chem.* **5** 397
Parsons R 1976 *Croat. Chem. Acta* **48** 597
Parsons R and Peat R 1980 *J. Res. Inst. Catal., Hokkaido Univ.* **28** 321
Parsons R and Peat R 1981 *J. Electroanal. Chem.* **122** 299
Parsons R, Peat R and Reeves R M 1975 *J. Electroanal. Chem.* **61** 151
Peat R and Shannon S 1983 *J. Electroanal. Chem.* **159** 229
Trasatti S 1970 *J. Electroanal. Chem.* **28** 257
Schiffrin D J 1969 *J. Electroanal. Chem.* **23** 168
Vos H, Wiersma J and Los J M 1974 *J. Electroanal. Chem.* **52** 27
Vos H and Los J M 1980 *J. Colloid Interface Sci.* **74** 360